Article | Received 13 September 2025; Revised 27 October 2025; Accepted 4 November 2025; Published 19 November 2025
https://doi.org/10.55092/opr20250002

Use of natural minerals toward cost-effective fabrication of layered structural colors by physical vapor deposition

Benjamin A. Rorem[1], Yian Cheng[2] and L. Jay Guo[1,2,*]

[1] Applied Physics, University of Michigan, Ann Arbor, Michigan 48109, USA
[2] Department of Electrical Engineering and Computer Science, University of Michigan, Ann Arbor, Michigan 48109, USA

* Correspondence author; E-mail: guo@umich.edu.

Highlights:

- Structural color coatings made from natural minerals via e-beam evaporation.
- Stable CuO-Fe_2O_3 optical absorbers enable vibrant, metal-free optical filters.
- Reproducible TiO_2 refractive indices achieved using ceramic powder sources.
- Optical performance validated by reflectance, ellipsometry, and XPS data.

Abstract: Structural color coatings offer exceptional vibrancy and durability but remain limited in many applications due to high material costs and fabrication complexity. This work aims to address the former limit and demonstrates multilayer optical coatings fabricated from un-processed natural mineral powders using electron beam evaporation. By using SiO_2 and TiO_2 based mineral materials as dielectric layers and a CuO–Fe_2O_3 mixture as an absorbing base, High-Low-Absorber (HLA) structures were fabricated that exhibit the desired reflection color. Refractive indices of TiO_2 films derived from ceramic powder are shown to be reproducible under controlled vacuum and source conditions, while the CuO–Fe_2O_3 mixture forms a stable film with high absorption and long-term conductivity. Structural colors deposited on both silicon and glass substrates exhibit strong agreement with optical simulations and are validated by reflectance spectra, ellipsometry, and X-ray photoelectron spectroscopy. This approach highlights a cost-effective pathway for producing optical coatings using minimally refined raw materials, with potential applications in photonics, optoelectronics, and sustainable color technologies.

Keywords: structural color coatings from natural minerals; High-Low-Absorber thin film design; electron beam evaporation of raw powders; thin-film interference; CuO-Fe_2O_3 absorbers; distillation; sustainable, low-cost, optical filters; ceramic powders

1. Introduction

Structural color coatings have drawn significant attention due to their unparalleled vibrancy, outstanding durability, and environmental resistance, providing distinct advantages over traditional organic pigment coatings in performance [1–16]. These coatings produce color through inorganic physical structures like

light interference in stacked thin films, rather than the absorption in chemical pigments, resulting in long-lasting colors that withstand UV radiation, humidity, temperature fluctuations, and chemical exposure [10,16–24]. Recent advancements in machine learning (ML) have revolutionized the design of optical coatings using a variety of material refractive indices, broadening their potential applications [25–29]. However, widespread use of structural color coatings is limited by the high cost of refined starting materials and vacuum-based deposition processes intended for electronic devices. In this work, we present an initial effort to tackle the first challenge by demonstrating that natural minerals, without refinement, can be used directly to produce interference-based structural colors by evaporation. We also note that solution-deposited layered structures have been developed to replace vacuum processes and have achieved a certain level of success in realizing various types of structures [19,30,31]. But thin films by physical vapor deposition still offer more precise control in film thickness and material refractive indices, two most important parameters in determining the resulting interference color.

This study explores the use of raw mineral powders to deposit thin films that achieve the optical properties required for structural color coatings. Ceramic powders and minerals such as SiO_2, TiO_2, CuO, and Fe_2O_3, as well as a mixed CuO-Fe_2O_3 system, are examined as potential evaporation source materials for making multilayer structures. Our focus is on materials that require minimal processing, as raw mineral powders can reduce both cost and environmental impact.

As a demonstration, we choose the High-Low-Absorber (HLA) structure, composed of three dielectric layers with distinct refractive indices, because it is particularly well-suited for testing different types of minerals for thin film-based structural colors [32]. In addition, the HLA design is capable of producing vibrant coatings without relying on high-purity refined metals as starting materials. In this work, SiO_2 and TiO_2 thin films serve as the low and high refractive index dielectrics, respectively, and a CuO-Fe_2O_3 mixture is developed as a stable light absorbing layer. The results demonstrate that ceramic powders can yield optical quality color coatings with reproducible properties; moreover, we observed that e-beam evaporation encourages the distillation and purification of these natural materials during deposition.

A range of structural colors are demonstrated using only ceramic powders and minerals, with optical properties confirmed through reflectance spectra, ellipsometry, and X-ray photoelectron spectroscopy (XPS). The CuO-Fe_2O_3 absorbing layer exhibits metallic-like absorption and electrical conductivity due to thermal-reduction during evaporation, confirmed by resistance measurements and XPS analysis of oxidation states and oxygen vacancies. This approach establishes a sustainable and cost-effective route for producing structural color coatings, suitable for applications in optoelectronics, protective coatings, and renewable energy.

2. Methods

2.1. Materials and film preparation

SiO_2, TiO_2, CuO, and Fe_2O_3 ceramic powders were obtained from US Pigment Corporation, with purities ranging from 95%–99% and particle sizes ranging from 10–50 μm. Scoria, blue topaz, and hematite were ground from raw mineral samples in a mortar & pestle and placed directly into crucible liners. 99.9% pure TiO_2 pellets were obtained from the Kurt J. Lesker company. Substrates included crystalline silicon wafers and glass slides, cleaned sequentially with acetone, isopropanol, and deionized water.

2.2. E-beam evaporation setup

Equipment: A Telemark electron beam evaporation control system was installed to a custom-built chamber and equipped with graphite crucible liners (4 cubic centimeters). The electron beam was emitted by a Telemark 244 e-beam source. The deposition controller was a Telemark 861, which measured the deposition rate with a quartz crystal sensor placed near the sample mount. E-beam power was controlled by the 861 and was represented as a percentage of the maximum power of the Telemark ST power supply. Substrates were at ambient temperature and rotated at 15 revolutions per minute by an external stepper motor.

Vacuum Conditions: Considering that natural minerals contain many impurities, we chose a fairly high chamber pressure of $5 \cdot 10^{-2}$ Pa during deposition as compared with that used in typical cleanroom e-beam evaporation processes. Vacuum is achieved with a Pfeiffer TMH 1001P turbo pump and a Leybold D25B rough pump. The pressure was monitored with a ZDF-5227A composite vacuum gauge.

Deposition Rates and Powers: In this study, natural minerals such as SiO_2, scoria, and blue topaz were deposited at a rate of 5 Å sec^{-1} at 9.5% power (9.6 kV, 0.028 A, 0.27 kW). TiO_2 was deposited at a rate of 3 Å sec^{-1} at 15% power (9.7 kV, 0.061 A, 0.59 kW). CuO was deposited at a rate of 0.3 Å sec^{-1} at 7.5% power (9.6 kV, 0.016 A, 0.15 kW). Fe_2O_3 and hematite gems were deposited at 0.5 Å sec^{-1} at 10% power (9.7 kV, 0.030 A, 0.29 kW). Higher deposition rate can be obtained by increasing the e-beam power.

Mixture Deposition: CuO and Fe_2O_3 powders were mixed in a 1:1 molar ratio before deposition. A uniform mixture encouraged the redox reaction when heated. The mixture was deposited at 3 Å sec^{-1} at 9% power (9.6 kV, 0.025A, 0.24 kW).

2.3. Optical and electrical characterization

Ellipsometry: Refractive indices and thicknesses were measured using a Woollam M-2000 Ellipsometer in the Lurie Nanofabrication Facility, with measurements taken between 300 and 1400 nm at 65, 70, and 75 degrees. All measured films were deposited on 300 nm SiO_2 on Si wafer pieces for ellipsometry measurement of the materials' refractive indices. All films except SiO_2 were modeled with a B-spline model. E2 was forced positive if the imaginary part of the index was negative. The Kramers-Kronig relation was used if it improved the goodness of fit. SiO_2 was modeled with a Cauchy model.

X-Ray Photoelectron Spectroscopy (XPS): XPS measurements were performed using a Kratos Axis Ultra DLD system with monochromatic Al kα source (10 mA, 12 kV) with a pass energy of 20 eV and a step size of 0.1 eV on a spot size of 700 μm by 300 μm. Spectra were recorded for the Cu 2p and Fe 2p regions, as well as the Cu LMM Auger peak. The obtained spectra were analyzed using CasaXPS software.

Optical spectrum characterization: Specular reflectance spectra at normal incidence were obtained using an Ocean Optics Inc. HR4000CG-UV-NIR High-Resolution Spectrometer integrated with a white light source.

Optical Microscopy: Optical microscope images were obtained with a Keyence VHX-7000 microscope at 50x magnification with full coaxial lighting.

Two-Point Resistance Measurement: Two-point resistance measurements were recorded with an Agilent 34401A digital multimeter. Standard leads and alligator clips were applied to the edges of the film, 2 cm apart.

2.4. Reflectance simulation

Simulated reflectance spectra were calculated using the Transfer Matrix Method approach in MATLAB. Optical constant data for the layers were measured with ellipsometry, described in the results section.

3. Results

3.1. Structural color coatings via HLA structures

Figure 1 demonstrates structural color coatings using an HLA design. Optical resonances are formed by light reflections between the HL and LA interfaces and constructive interference. Each coating consists of a 40 nm high refractive index TiO_2 top layer and a lower index variable-thickness SiO_2 cavity layer deposited on a crystalline silicon substrate. Both films were deposited using ceramic powder sources, in contrast with high-purity e-beam pellets.

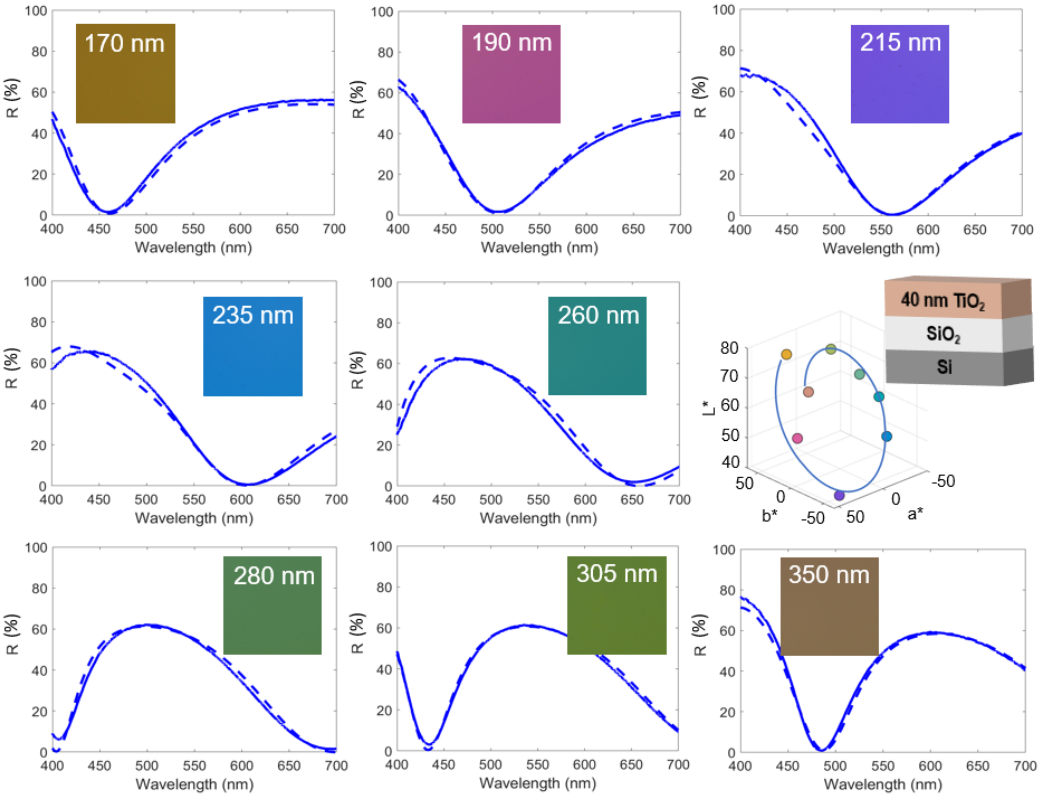

Figure 1. High-chroma, planar HLA coatings with varying SiO_2 cavity thicknesses. Figures show the measured (solid line) and simulated (dashed line) optical reflectance spectra (*i.e.* R *vs.* wavelength), and the corresponding colors and SiO_2 cavity thickness are shown as insets. These insets are optical microscope images of evaporated HLA coatings (2 × 2 mm). The simulated spectra were obtained through the transfer matrix method using measured refractive indices of the evaporated mineral films. Both TiO_2 and SiO_2 layers were deposited using ceramic powder sources, and the substrate was crystalline silicon. CIEL*a*b* coordinates for the coatings are shown on the right.

By varying the SiO_2 cavity thickness from 170 to 350 nm, a wide array of colors ranging from yellow to purple to green was produced. Reflectance spectra, both measured and simulated, are provided for each color in Figure 1, along with optical microscope images of 2 × 2 mm color-coated regions

shown in the inset. Simulations were performed using the transfer matrix method (TMM) and refractive index data obtained from spectroscopic ellipsometry. Measured and simulated reflection spectra showed close agreement, with simulated reflection peaks exhibiting $\Delta R = 2\%$ and $\Delta\lambda = 2$ nm on average, while the measured peaks showed slightly larger variations of $\Delta R = 4\%$ and $\Delta\lambda = 5$ nm on average. Corresponding CIEL*a*b* coordinates are shown on the right, representing the lightness, chroma, and hue of each coating.

These results highlight that vibrant, high-chroma colors can be achieved using low-cost ceramic powders with minimal processing. The spiral pattern in the a*b* space indicates that chroma decreases as the SiO_2 thickness increases. All optical microscope images were captured at 50 × magnification with full coaxial lighting, and each color spans a 2 × 2 mm region.

In this proof-of-principle example, the silicon substrate was used as an absorber for easy ellipsometry and reflectance measurements. To deposit on arbitrary substrates, such as glass or plastic, an alternative absorbing base layer is required. Later sections explore candidate absorber layers to expand the structural color platform to more practical surfaces.

3.2. Reproducibility and index control of TiO_2/SiO_2 films

The optical refractive indices of TiO_2 films deposited under various conditions are shown in Figure 2a. The red curve corresponds to a film deposited in a cleanroom e-beam evaporator using 99.9% pure TiO_2 pellets. The green and blue curves represent films deposited in our custom-built evaporator using either pure pellets (green) or ceramic powder (blue). The high purity pellets' refractive index was higher in the cleanroom compared to our chamber due to a lower chamber pressure resulting in a denser film, and possibly higher oxygen content in the film deposited in our custom evaporator operating under much higher base pressure. All three samples show similar refractive index shape across the visible spectrum. The inset displays the imaginary part (k), which remains low for all samples, indicating minimal absorption.

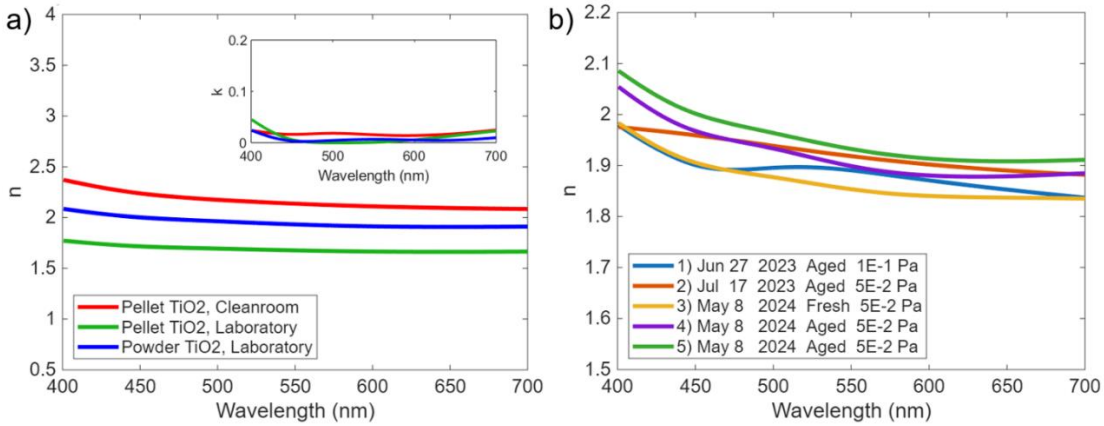

Figure 2. Optical refractive index of TiO_2 under various deposition conditions. **(a)** The real part of the complex refractive index, n, of TiO_2 deposited in a cleanroom evaporator (red) and laboratory evaporator (green and blue). The cleanroom sample used pure pellets, while the laboratory samples used either pure pellets or ceramic powder. The inset shows the imaginary refractive index, k, for the same samples, showing minimal absorption across the visible spectrum; **(b)** The real part of the complex refractive index of TiO_2 deposited in the laboratory evaporator, measured multiple times to demonstrate stability. All samples were deposited using ceramic powder. The yellow and green samples were deposited on the same day, but the yellow sample was deposited with fresh powder.

To further assess reproducibility, five additional TiO_2 samples were deposited under controlled conditions using ceramic powder. The real part of their complex refractive indices are shown in Figure 2b. The maximum variation in refractive index is approximately 0.1, with differences arising from the vacuum level and the state of the crucible material. For example, sample 1 was deposited at a higher pressure (~10^{-1} Pa), while samples 3 and 5 were deposited at ~$5 \cdot 10^{-2}$ Pa. As a result, sample 1 has a lower film density and lower refractive index. The state of the crucible material is a factor, too; sample 5 used aged crucible material, whereas sample 3 used fresh powder. Reduced titanium oxide species, such as Ti_3O_5, form over time in the crucible material, due to oxygen loss during evaporation. Ti_3O_5 has a slightly lower melting point (1777 °C) and a higher refractive index than TiO_2 (melting point 1855 °C), making it more volatile and more likely to be deposited [33]. Thus, films with an aged crucible material will tend to have a higher refractive index than fresh crucibles. To maintain consistent refractive indices, a constant chamber pressure and regular crucible replenishment are needed. These results show that ceramic powder, despite many impurities and being deposited at higher base pressure, can produce TiO_2 films with consistent refractive indices like those made from high-purity materials. This demonstrates that low-cost powders can be used for optical-quality color coatings.

3.3. Absorbing film development: CuO, Fe_2O_3, and their mixture

Two mineral materials, CuO and Fe_2O_3, were examined as potential absorbing layers for the HLA structure. Each was deposited from ceramic powders derived from tenorite and hematite, respectively. The refractive indices for the resulting thin films are shown in Figure 3, including measurements taken after exposure to ambient air for multiple days. It turns out that, individually, neither of these two minerals can function as a useful absorber material to give consistent results due to instability during film deposition.

CuO and Fe_2O_3 display different optical properties to TiO_2 and SiO_2, introduced earlier. The CuO film (blue curve) displayed significant optical absorption yet a notable index shift over time, indicating post-deposition oxidation in air. In contrast, the Fe_2O_3 film (cyan) was stable in air; however, the residual melt in the crucible became magnetic after cooling, suggesting a phase change during evaporation. These results indicate that both CuO and Fe_2O_3 undergo reduction reactions during deposition but may lack long-term stability when used individually, as copper and iron tend to return to higher oxidative states in ambient air environment. A mixture of CuO and Fe_2O_3 powders in a 1:1 molar ratio was deposited to investigate potential redox interactions. The resulting film exhibited a distinct optical response, with refractive indices resembling those of metallic copper (Figure 3, black curve). Two-point resistance measurements taken five months after deposition showed a value of 220 Ω across a 2 cm span, confirming the film's metallic behavior and long-term stability. Although minor index shifts were observed with air exposure, they were smaller than those of CuO alone.

We found that this mixed-oxide film offers two key advantages over individual CuO or Fe_2O_3 layers: (1) improved film absorption stability and (2) higher deposition rates without spitting or thermal instability. The mixture also displayed a liquid phase, unlike the solid phases of the two individual oxides, with the appearance of molten copper during evaporation. Molten copper metal, with high thermal conductivity, may explain why the deposition is stable without spitting.

To gain further insight into the chemical states present in the films, X-ray Photoelectron Spectroscopy (XPS) analysis (Figure 4a–d) was conducted. The Cu 2p and O 1s spectra of the fresh CuO

film (red) revealed primarily Cu(I) species with a singlet oxygen peak, while the aged film (blue) showed the presence of both Cu(I) and Cu(II), confirming progressive oxidation [34]. The CuO-Fe_2O_3 mixture (green) displayed Cu(0)/Cu(I) features, including teeth-like Auger spectra peaks consistent with metallic copper [35]. These results are consistent with the optical data and confirm the presence of reduced copper species in the mixed-oxide film.

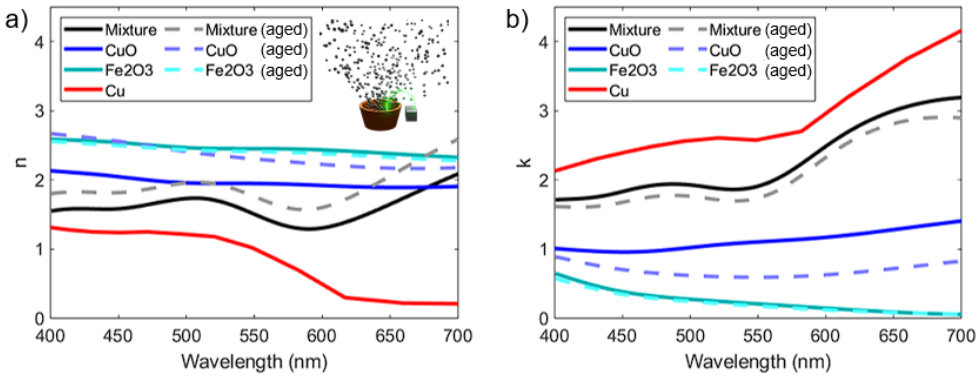

Figure 3. Optical refractive indices of absorbing thin films, including the **(a)** real and **(b)** imaginary parts. The refractive index for evaporated copper metal (red) is shown, while the other films—CuO, Fe_2O_3, and the CuO-Fe_2O_3 mixture – were deposited using ceramic powders in a private e-beam evaporator. Solid lines represent fresh films, and dashed lines indicate aged, 5-day-old films, with changes observed in CuO and the mixture.

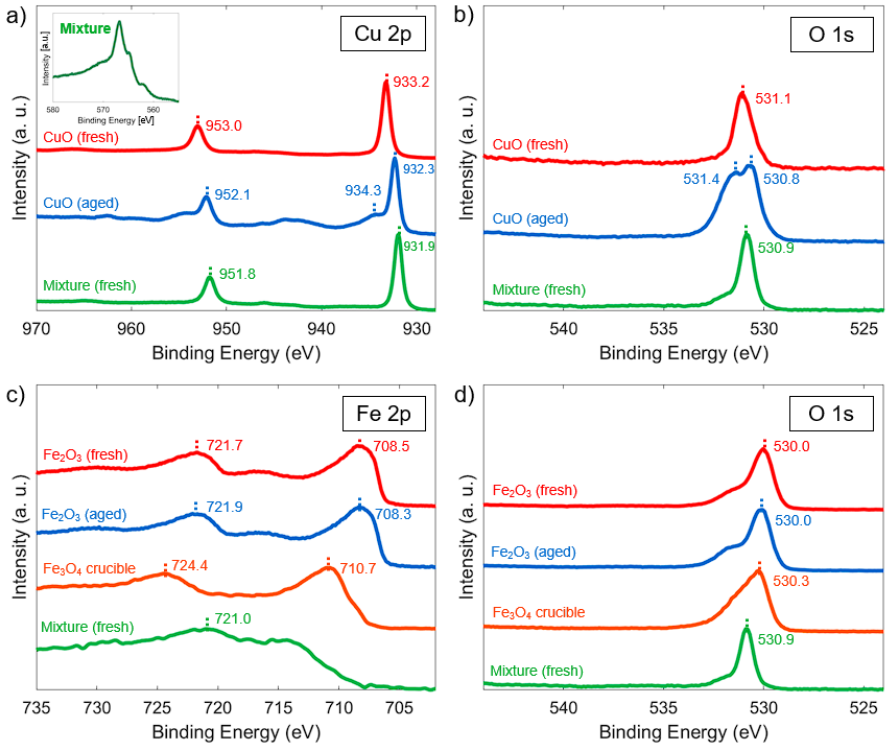

Figure 4. XPS spectra of copper oxide and iron oxide thin films. **(a)** Cu 2p and **(b)** O 1s spectra for copper oxide films, and **(c)** Fe 2p and **(d)** O 1s spectra for iron oxide films. Each film was approximately 20 nm thick. Fresh films (red) were exposed to atmosphere for 30 minutes, while aged films (blue) were exposed to atmosphere for five days. The film deposited from the CuO-Fe_2O_3 mixture (green) in **(a)** includes an Auger LMM spectrum. The Fe_3O_4 crucible sample (orange) is also shown in **(c)** and **(d)**. Peak binding energies are labeled in each plot.

The iron oxide films also illuminate some material changes during deposition. In Figure 4c–d, the Fe 2p and O 1s spectra are shown for fresh and aged iron oxide films, indicating no progressive oxidation in the deposited films. Despite this, the crucible melt spectrum matches Fe_3O_4, a reduced iron oxide. Due to the distillation effect during evaporation, Fe_2O_3 tends to evaporate before Fe_3O_4, resulting in an increasing concentration of Fe_3O_4 compounds in the crucible melt. As for the CuO-Fe_2O_3 mixture, the Fe 2p signal was weak. Again, this is likely due to distillation and the higher melting temperatures of iron oxides compared to copper oxides, indicating a low iron content in the final film [36–38]. These results reveal that the mixture deposits as a metallic copper oxide film with minimal iron oxide presence.

Together, the optical, electrical, and spectroscopic results demonstrate that the CuO-Fe_2O_3 mixture yields a stable, highly absorbing thin film suitable for use as the bottom layer in the HLA structure. This mixture serves as a low cost alternative to conventional absorbing materials and allows structural color coatings to be deposited on arbitrary substrates, including glass and plastic.

3.4. Full HLA structures on arbitrary substrates

With the CuO–Fe_2O_3 mixture identified as a stable absorbing layer, full HLA structures were fabricated on transparent glass substrates. Each coating consisted of a 100 nm CuO–Fe_2O_3 base layer, a variable-thickness SiO_2 cavity layer, and a 40 nm TiO_2 top layer. All three layers were deposited from ceramic powder sources using e-beam evaporation. Optical microscope images of the resulting color coatings are shown in Figure 5, each covering a 2 × 2 mm area.

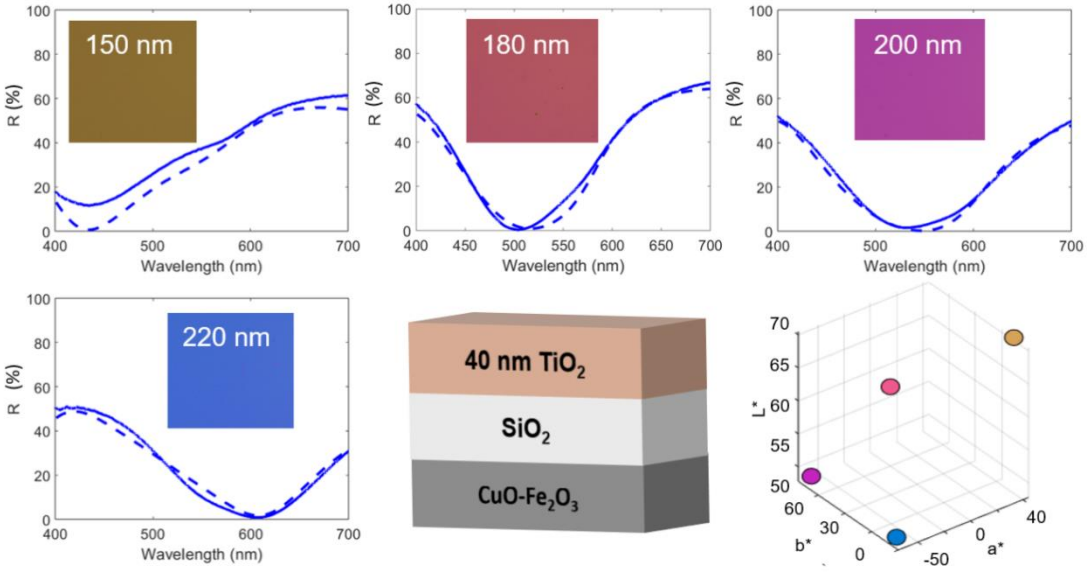

Figure 5. High-chroma HLA color coatings on a mixed CuO-Fe_2O_3 absorber base. Figures show the measured (solid line) and simulated (dashed line) reflection spectra of four coatings, with optical microscope images (2 × 2 mm) and the SiO_2 cavity thickness as insets. The structure consists of a 40 nm TiO_2 layer on an SiO_2 layer atop a 100 nm CuO-Fe_2O_3 layer deposited on a glass substrate. TiO_2, SiO_2, and CuO-Fe_2O_3 layers were deposited using ceramic powder sources. Simulated spectra were generated with the transfer matrix method using measured refractive indices of evaporated films. CIEL*a*b* coordinates for each color are shown on the right. The CIEL*a*b* coordinates show similar chroma and lightness to the HLA structures in Figure 1.

As in earlier demonstrations on silicon, varying the SiO_2 cavity thickness produced a wide range of vibrant structural colors. The measured and simulated reflectance spectra for each structure are included in Figure 5, along with the corresponding CIEL*a*b* coordinates. These coatings achieved reflection peaks of approximately 60%, similar to those obtained using silicon substrates.

Simulations were performed using the transfer matrix method (TMM), with optical constants obtained by ellipsometry. Quantitative comparison between measured and simulated reflection spectra shows mostly agreement, with an average simulated reflection peak uncertainty of $\Delta R = 8\%$ and $\Delta\lambda = 7$ nm and an average measurement peak uncertainty of $\Delta R = 10\%$ and $\Delta\lambda = 8$ nm. A complete comparison with the samples from Figure 1 is shown in Table 1. Differences between measured and simulated reflectance spectra were primarily attributed to variation in the optical constants of the absorbing layer, as shown in Figure 3. The index fluctuations of the $CuO–Fe_2O_3$ mixture resulted in a maximum reflectance deviation of approximately 10%.

The successful demonstration of structural color coatings on glass substrates using fully mineral-derived layers highlights the practicality of this method for a wide range of surfaces. In this way, the HLA design can be extended to transparent or flexible substrates for broader applications in optics and photonics.

Table 1. Comparison of reflected peak uncertainties between measurement and simulation.

Samples	ΔR (%)	Δλ (nm)
HLA on Silicon, Measurements	4	5
HLA on Silicon, TMM Simulations	2	2
HLA on Glass, Measurements	10	8
HLA on Glass, TMM Simulations	8	7

3.5. E-beam evaporation with raw materials and best practices

E-beam evaporation was selected for this work due to its unique capability to process solid powders with mixed compositions and variable purities. Compared to other physical vapor deposition methods, such as sputtering (requiring pre-fabricated sputter targets) or pulsed laser deposition, e-beam evaporation can melt and refine ceramic powders *in situ*, allowing for thin film fabrication directly from natural minerals.

Several key practices were identified to ensure high-quality and repeatable deposition results when using raw materials. Maintaining a stable vacuum level during deposition is critical, as the presence of air molecules affects film packing density and oxygen concentration, thus, optical properties like refractive index. In this study, a chamber pressure of approximately $5 \cdot 10^{-2}$ Pa was used, which provided adequate deposition conditions while reducing the need for high-vacuum typically required for electronic-grade coatings. Repeatable deposition quality also requires regular crucible material replenishment since the composition changes over time due to distillation.

Materials with low thermal conductivity, such as ceramic powders, require gentle heating to avoid large thermal gradients and spitting. Beam sweeping was employed to distribute heat and reduce localized boiling. Additionally, consistent crucible preparation and regular replacement of aged material helped ensure uniform deposition rates and refractive indices, particularly for sensitive materials like TiO_2.

In many cases, e-beam evaporation refined the source material through distillation, a purification process involving vapor phase separation [39]. For example, scoria and blue topaz, despite containing

metal oxides and impurities, produced SiO_2-like films due to the higher vapor pressure of silica relative to the other components. Similarly, the $CuO–Fe_2O_3$ mixture underwent redox reactions during heating, resulting in partial reduction of CuO to Cu metal, as confirmed by optical and XPS data. These observations highlight the importance of vapor pressure and thermodynamic stability in determining the final film composition.

The combined effects of thermal decomposition, redox reactions, and distillation enable e-beam evaporation to not only deposit thin films from raw materials but also purify them during the process. When paired with the HLA design, this approach supports scalable and sustainable structural color coatings with minimal material refinement.

4. Conclusion

This work demonstrates that vibrant structural color coatings can be fabricated using raw mineral-derived films deposited by electron beam evaporation. The High-Low-Absorber (HLA) structure serves as an effective platform for showcasing optical quality and reproducibility using minimally refined ceramic powders.

SiO_2 and TiO_2 thin films produced from ceramic powders matched the optical performance of their high-purity counterparts, with repeatable refractive indices under controlled vacuum and source material conditions. To extend the applicability of the HLA structure to arbitrary substrates, a $CuO–Fe_2O_3$ mixture was developed as a cost-effective absorbing layer. This film exhibited stable metallic-like absorption and electrical conductivity, confirmed through ellipsometry, 2-point resistance measurements, and X-ray photoelectron spectroscopy.

Mineral-based HLA coatings demonstrated vivid colors with reflection peaks at 60% and peak uncertainties of $\Delta R = 10\%$ and $\Delta\lambda = 8$ nm, agreeing well with simulations. Key contributors to measurement uncertainty were the variations in deposition chamber pressure and the age of the crucible melt. Uncertainty in simulations was due to variations in film optical constants.

The use of raw mineral powders in e-beam evaporation enabled *in situ* refinement through distillation and redox reactions, allowing for the formation of stable thin films from complex source mixtures. Together, these findings establish a practical and scalable route for producing structural color coatings with significantly reduced material costs and environmental impact.

Structural color coatings made from e-beam evaporation of abundant natural minerals offer a promising and cost-effective alternative to refined materials. The results presented here support the broader development of optical coatings for sustainable photonics, including applications in optoelectronics, display technology, and environmentally robust surface treatments. Future efforts may include integrating these coatings into functional devices and expanding the material palette through machine-learning-guided design.

5. Lessons learned

A key insight from this work is that the optical properties of bulk materials, including color and refractive index, do not directly translate to the behavior of their evaporated thin film counterparts. Early experiments using ground scoria and blue topaz powders revealed that despite vibrant bulk coloration, the resulting films appeared translucent or colorless under visible light with flat refractive index profiles. This discrepancy was attributed to two primary factors: (1) the low absorption coefficients of these materials

once reduced to nanoscale thicknesses, and (2) reduction and distillation during high-temperature evaporation. These findings resulted in a necessary pivot in our material selection strategy—prioritizing ceramic sources that yielded stable and optically functional films after deposition. While these results were ultimately omitted from the main discussion for focus and clarity, they provided a critical foundation for identifying CuO and Fe_2O_3 as viable absorbers.

Another important lesson was learned from our efforts to achieve reproducible refractive indices, particularly for TiO_2. Despite the use of impure ceramic powders and crucibles prone to contamination, we observed that consistent vacuum conditions and control over deposition rate and crucible geometry led to repeatable optical constants. Our results suggest that, under proper conditions, evaporated films deposit with repeatable optical quality, even when starting with minimally processed mineral sources.

Finally, this work benefited from several practical refinements in e-beam process engineering. For example, the use of graphite crucibles improved film purity for TiO_2 but may have been detrimental for CuO, where partial reduction to Cu_2O or metallic copper occurred. This issue can be solved with two approaches. (1) A different crucible material, such as alumina, can provide more chemical stability for some molten materials. While this is a good technique, the more interesting solution is the second approach. (2) Replacing a single material source with pre-mixed absorbers also improved layer uniformity and stability, as we discovered that co-evaporating copper and iron oxides produced a metallic-like film that avoided common aging and deposition issues. These iterative adjustments, though not always immediately successful, collectively enabled reliable fabrication of vibrant, scalable, and metal-free structural color coatings.

Acknowledgments

This work is supported by the National Science Foundation under Grant No. PFI-2213684. The authors also acknowledge the financial support of the University of Michigan College of Engineering and technical support from the Michigan Center for Materials Characterization and the Lurie Nanofabrication Facility. BR would also like to acknowledge Dennis Schweiger and Matthew Oonk for evaporation assistance; Daniel Penley for microscope imaging.

Authors' contribution

Conceptualization, LG; methodology, BR and LG; software, BR and YC; validation, BR, YC, and LG; formal analysis, BR; data curation, BR; writing—original draft preparation, BR; writing—review and editing, BR, YC, and LG; visualization, BR and LG; supervision, LG; project administration, LG; funding acquisition, LG. All authors have read and agreed to the published version of the manuscript.

Conflicts of interests

Prof. L. Jay Guo holds the position of Editor-in-chief for *Optics and Photonics Research* and has not peer reviewed or made any editorial decisions for this paper.

References

[1] Arsenault AC, Puzzo DP, Manners I, Ozin GA. Photonic-crystal full-colour displays. *Nat. Photonics* 2007, 1(8):468–472.

[2] Hong J, Chan E, Chang T, Fung TC, Hong B, *et al.* Continuous color reflective displays using interferometric absorption. *Optica* 2015, 2(7):589.

[3] Zhu X, Vannahme C, Højlund-Nielsen E, Mortensen NA, Kristensen A. Plasmonic colour laser printing. *Nat. Nanotechnol*. 2016, 11(4):325–329.

[4] Kumar K, Duan H, Hegde RS, Koh SCW, Wei JN, *et al*. Printing colour at the optical diffraction limit. *Nat. Nanotechnol*. 2012, 7(9):557–561.

[5] Kim H, Ge J, Kim J, Choi SE, Lee H, *et al.* Structural colour printing using a magnetically tunable and lithographically fixable photonic crystal. *Nat. Photonics* 2009, 3(9):534–540.

[6] Lee KT, Ji C, Banerjee D, Guo LJ. Angular- and polarization-independent structural colors based on 1D photonic crystals. *Laser Photon Rev*. 2015, 9(3):354–362.

[7] Banerjee D, Zhang M. Quarter-wave design criteria for omnidirectional structural colors. *J. Mod. Opt.* 2010, 57(13):1180–1188.

[8] Masuda T, Kudo Y, Banerjee D. Visually attractive and high-power-retention solar modules by coloring with automotive paints. *Coatings* 2018, 8(8):282.

[9] Masuda T, Hirai S, Inoue M, Chantana J, Kudo Y, *et al.* Colorful, flexible, and lightweight Cu(In,Ga)Se2 solar cell by lift-off process with automotive painting. *IEEE J. Photovolt.* 2018, 8(5):1326–1330.

[10] Ji C, Lee KT, Xu T, Zhou J, Park HJ, *et al.* Engineering light at the nanoscale: structural color filters and broadband perfect absorbers. *Adv. Optical Mater*. 2017, 5:1700368.

[11] Xu G, Shen L, Cui C, Wen S, Xue R, *et al.* High-performance colorful semitransparent polymer solar cells with ultrathin hybrid-metal electrodes and fine-tuned dielectric mirrors. *Adv. Funct. Mater*. 2017, 27(15):1605908.

[12] Lu J, Lin Y, Jiang B, Yeh CH, Kao J, *et al.* Microcavity structure provides high-performance (> 8.1%) semitransparent and colorful organic photovoltaics. *Adv. Funct. Mater*. 2018, 28(7):1703398.

[13] Ji C, Zhang Z, Masuda T, Kudo Y, Guo LJ. Vivid-colored silicon solar panels with high efficiency and non-iridescent appearance. *Nanoscale Horiz*. 2019, 4(4):874–880.

[14] Sabnis RW. Color filter technology for liquid crystal displays. *Displays* 1999, 20:119–129.

[15] Li Z, Butun S, Aydin K. Large-area, lithography-free super absorbers and color filters at visible frequencies using ultrathin metallic films. *ACS Photonics* 2015, 2(2):183–188.

[16] Rorem BA, Cho TH, Farjam N, Lenef JD, Barton K, *et al.* Integrating structural colors with additive manufacturing using atomic layer deposition. *ACS Appl. Mater. Interfaces* 2022, 14(27):31099–31108.

[17] Shi X, He J, Lu X. Functional structural color dye with excellent UV protection property. *Dyes Pigm.* 2020, 175:108142.

[18] Ji C, Lee KT, Guo LJ. High-color-purity, angle-invariant, and bidirectional structural colors based on higher-order resonances. *Opt. Lett.* 2019, 44(1):86.

[19] Ji C, Acharya S, Yamada K, Maldonado S, Guo LJ. Electrodeposition of large area, angle-insensitive multilayered structural colors. *ACS Appl. Mater. Interfaces* 2019, 11(32):29065–29071.

[20] Wang H, Zhang K. Photonic crystal structures with tunable structure color as colorimetric sensors. *Sensors* 2013, 13:4192–4213.
[21] Lee HS, Shim TS, Hwang H, Yang S, Kim SH. Colloidal photonic crystals toward structural color palettes for security materials. *Chem. Mater.* 2013, 25(13):2684–2690.
[22] Sun J, Bhushan B, Tong J. Structural coloration in nature. *RSC Adv.* 2013, 3(35):14862–14889.
[23] Xu T, Shi H, Wu Y, Kaplan AF, Ok JG, *et al.* Structural colors: from plasmonic to carbon nanostructures. *Small* 2011, 7(22):3128–3136.
[24] Yang C, Shen W, Zhang Y, Li K, Fang X, *et al.* Compact multilayer film structure for angle insensitive color filtering. *Sci. Rep.* 2015, 5(1):9285.
[25] Wang H, Guo LJ. NEUTRON: neural particle swarm optimization for material-aware inverse design of structural color. *IScience* 2022, 25(5):104339.
[26] Wang H, Zheng Z, Ji C, Guo LJ. Automated multi-layer optical design via deep reinforcement learning. *Mach. Learn. Sci. Technol*. 2021, 2(2):025013.
[27] Ma T, Wang H, Guo LJ. OptoGPT: a foundation model for inverse design in optical multilayer thin film structures. *Opto-Electron. Adv.* 2024, 7(7):240062.
[28] Saha A, Ma T, Wang H, Guo LJ. Environmentally sustainable and multifunctional chrome-like coatings having no chromium designed with reinforcement learning. *ACS Appl. Mater. Interfaces* 2023, 15(23):28772–28780.
[29] Wang D, Liu Z, Wang H, Li M, Guo LJ, *et al.* Structural color generation: from layered thin films to optical metasurfaces. *Nanophotonics* 2023, 12:1019–1081.
[30] Feng W. Multilayer structural colors realized by solution-based fabrications. Doctoral Thesis, University of Michigan, 2023.
[31] Feng W, Paik J, Guo LJ. Solution-processed structural colors and their applications. *Mater. Chem. Front.* 2024, 8:3474–3508.
[32] Feng W, Cheng Y, Guo LJ. Temporal coupled mode analysis of chromaticity in trilayer subtractive structural colors. *ACS Photonics* 2023, 10(8):2784–2792.
[33] Lide DR. *CRC Handbook of Chemistry and Physics*, 79th ed. Boca Raton: CRC Press, 1998.
[34] Pauly N, Tougaard S, Yubero F. Determination of the Cu 2p primary excitation spectra for Cu, Cu 2O and CuO. *Surf Sci*. 2014, 620:17–22.
[35] Biesinger MC. Advanced analysis of copper X-ray photoelectron spectra. *Surf. Interface Anal.* 2017, 49(13):1325–1334.
[36] Al-Kuhaili MF, Saleem M, Durrani SMA. Optical properties of iron oxide (α-Fe 2O 3) thin films deposited by the reactive evaporation of iron. *J. Alloys Compd*. 2012, 521:178–182.
[37] Yamashita T, Hayes P. Analysis of XPS spectra of Fe 2+ and Fe 3+ ions in oxide materials. *Appl. Surf. Sci.* 2008, 254(8):2441–2449.
[38] Mills P, Sullivan JL. A study of the core level electrons in iron and its three oxides by means of X-ray photoelectron spectroscopy. *J. Phys. D: Appl. Phys.* 1983, 16(5):723.
[39] Speight JG. *The Chemistry and Technology of Petroleum*. Boca Raton: CRC Press, 2006.